Rivista Italiana di Paleontologia e Stratigrafia
(*Research in Paleontology and Stratigraphy*)
vol. 130(2): 475-486. **July 2024**
DOI: https://doi.org/10.54103/2039-4942/21688

MIRAGAIA TAIL BIOMECHANICS AND DEFENCES. EVALUATION OF THE TAIL MOBILITY AND RESISTANCE TO LOADINGS AND COLLISIONS.

FRANCESCO LATEGANO[1], SIMONE CONTI[2,3] & FRANCESCA LOZAR[1]

[1]Università degli Studi di Torino, Dipartimento di Scienze della Terra, Via Valperga Caluso, 35, 10125 Torino.
E-mail: fncltg@gmail.com - francesca.lozar@unito.it
[2]GEOBIOTEC, Department of Earth Sciences, NOVA School of Science and Technology, Campus de Caparica, P-2829 516 Caparica, Portugal.
[3]Department of Aerospace Science and Technology, Politecnico di Milano, Milano, Italy, via La Masa 34, 20156, Milano, Italy.
E-mail: conti.simone.1994@gmail.com

Associate Editor: Silvio Renesto.

To cite this article: Lategano F., Conti S. & Lozar F. (2024) - *Miragaia* tail biomechanics and defences. Evaluation of the tail mobility and resistance to loadings and collisions. *Riv. It. Paleontol. Strat.*, 130(2): 475-486.

Keywords: Stegosaurs; MBDA; *Miragaia longicollum*; thagomizer; tail weaponization.

Abstract. Thyreophora is a taxon of dinosaurs composed of Stegosauria and Ankylosauria, whose members have been known to utilise their tails as powerful defensive weapons. Remains of these dinosaurs are scarce; the Portuguese taxon, *Miragaia longicollum*, known from three individuals, provides precious pieces of information on the anatomy of these rare animals. This study estimates the stress resistance of a stegosaurian tail and uses Multi-Body Dynamics Analysis (MBDA) to properly simulate the movements of the tail of *M. longicollum*. The results show that the tail of *M. longicollum* can achieve high speeds and generate significant pressures, akin to those observed in other tyreophoran dinosaurs. Such high speeds would potentially generate powerful strikes and would inflict injuries on predators. However, the caudal spines of *M. longicollum*, despite being larger than those of *Stegosaurus stenops*, have worse stress-bearing performances than those of *S. stenops*, due to their different morphology. Investigating the complex biomechanics governing the tail of a dinosaur, such as *M. longicollum*, can have significant implications across various disciplines. Investigating biomechanics in extinct species offers valuable insights into comparative anatomy and physiology, facilitating connections between ancient and contemporary life forms. Palaeontologists and evolutionary biologists might use this information to better comprehend the dinosaur movement, which would advance our understanding of ancient ecosystems and have an impact on how we interpret the behaviour of contemporary animals. The knowledge obtained from such study might provide useful biomimicry lessons for robotics engineers, serving as inspiration for the creation of more adaptable and agile robotic systems.

Received: November 18, 2023; accepted: July 17, 2024

Introduction

Stegosauria is a suborder of armoured herbivorous ornithischian dinosaurs that is part of the clade Thyreophora, the sister taxon to Ankylosauria; it was named after the earliest recognised species, *Stegosaurus stenops* (Marsh, 1887). Stegosaur dinosaurs have been recovered in present-day North America, Europe, Asia, and Africa, from sites dating from the Early to the Late Jurassic; they become scarcer in the Early Cretaceous from Siberia (Marsh 1887; Averianov & Krasnolutskii 2009; Mallison 2015; Costa & Mateus 2019; Jia et al. 2024; Li et al. 2024; Zafati et al. 2024); the youngest remains possibly date to the Late Cretaceous of India (Galton & Ayyasami 2017), and China (Jia et al. 2024; Li et al. 2024). The stegosaur remains found in Europe have been historically attributed to *Dacentrurus armatus* (Owen, 1875) until it was possible to identify the fossils of *Miragaia longicollum* (Mateus et al., 2009) as belonging to a new genus and species of dinosaur. The remains of *M. longicollum* were uncovered in Upper Jurassic rocks belonging to the Lourinhã Formation cropping out in Western Portugal. The name of the genus comes from the adjacent settlement of "Miragaia", which means "wonderful goddess of the Earth," while the species name comes from the Latin term *longicollum*, meaning "long neck". The species name reveals one of the autapomorphies of the genus, which is the possession of 17 cervical vertebrae, thus possessing the most elongated neck among Stegosauria (Costa & Mateus 2019). To date, the remains of three individuals have been described, and all have been recovered from strata of the Lourinhã Formation in Portugal (Mateus et al. 2009; Costa & Mateus 2019), allowing a nearly complete reconstruction of the animal. The last described specimen, MG 4863, remarkably preserves an almost intact tail, including 25 caudal vertebrae and one caudal spine; this facilitate the acquisition of essential data required to conduct computer simulations and explore its dynamic properties. Another feature characteristic of *M. longicollum* is the sigmoid shape of the cross section of the caudal spines (Costa & Mateus 2019*,* Fig. 68*),* different in comparison to the ellipsoid shape of the caudal spines of *S. stenops* (Marsh 1887; Carpenter et al. 2005; Maidment et al. 2015).

Different approaches have been employed in studying the dinosaur tail motion, (Gertsch 1994; Arbour & Zanno 2018 and references therein). Among them stands Multibody Dynamics Analysis (MBDA), which has been used in the present as well as in former (Mallison 2011) studies. MBDA is a technique employed in several scientific disciplines, including aerospace, building, and automotive engineering, to evaluate the motion of intricate mechanical systems (Langenbach et al. 2002; Curtis et al. 2008; Moazen et al. 2008; Lautenschlager 2020). In this context, Multibody Dynamics Analysis (MBDA) stands out as a pivotal tool for investigating the biomechanics and dynamics of extinct species. Given some simplifications, the skeleton of vertebrates can be compared to a complex system of interconnecting rigid components coupled with kinematic restrictions and lasting stresses. The caudal axial muscles, which are further subdivided into epaxial and hypaxial muscles, control the mobility of the tail and hindlimbs (Hutchinson et al. 2019; Díez Díaz et al. 2020). MBDA has already been applied to estimate the tail dynamics and behavioural patterns of several groups of dinosaurs (Mallison 2015; Conti et al. 2020; Van Bijlert et al. 2021). It aids understanding the function and development of various anatomical features and behaviours, that could never be tested otherwise (Lautenschlager 2020). Thyreophora, along with some Sauropoda members (e.g. *Shunosaurus lii,* Dong et al. 1983), is the dinosaur group that has demonstrated tail weaponisation (Bakker 1986; Carpenter et al. 2005; Arbour 2009). The hypothesis that stegosaurian dinosaurs could be able to use their tails for defence was advanced since the first findings (Marsh 1880; Lull 1910). Studies such as Gilmore (1914) and Janensch (1925) have contested its validity, suggesting that the vertebral column may have lacked the necessary flexibility for effective defensive purposes. Direct evidence in favour of tail-blow-inflicted damage is necessarily scant. Yet, a caudal vertebra from *Allosaurus fragilis* (specimen UMNH 10781) revealed a pathology affecting the caudal rib, compatible with the morphology of a caudal spine of *Stegosaurus stenops* (Carpenter et al. 2005). The initial application of MDBA to stegosaurian dinosaurs, exemplified by the study of *Kentrosaurus aethiopicus*, involved quantifying the range of motion of its tail and simulating its movement to explore defensive capabilities (Mallison 2011). In this work, we apply MBDA analysis to answer the question of whether *M. longicollum* could have utilised its tail and caudal spines as a weapon.

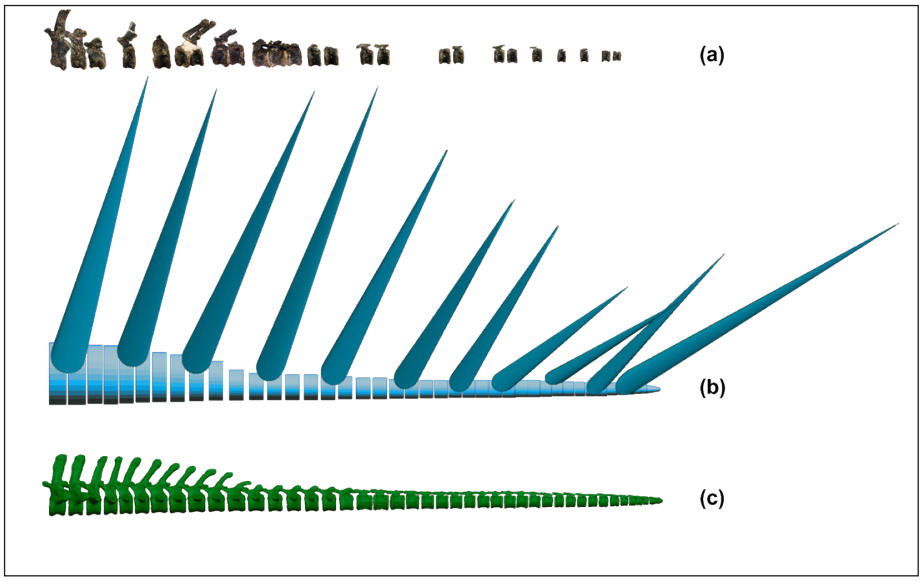

Fig. 1 - Photographic material of the tail modified from Costa and Mateus (2019) (a); geometric model used by the software MBDyn (b); model used in the visual reconstruction (c).

Materials and methods

The simulation model is based on the fossils referred to as MG 4863. Data were collected from published information on this specimen (Costa & Mateus 2019) and the missing elements were statistically calculated using the maximum likelihood method (Kang 2013) to complete the model (Fig. 1). The thickness of the articular cartilages is estimated to range between 15% and 12% of the length of the consecutive element (Fig. 2), as suggested by previous studies (Díez Díaz et al. 2020). The total number of tail elements for *M. longicollum* is unknown, with 25 preserved elements reaching up to the 37th position, and five more hypothesised missing elements (Fig. 1; Costa & Mateus 2019). Thus, the model comprises 42 cylinders, each representing a caudal vertebra, and 22 cones, each representing a caudal spine (Fig. 1). Hinge joints intersperse each cylinder, to simulate the action of the articulation between bones; and a deformable joint superimposes each hinge joint, to simulate the action of ligaments and bones. The deformable joints are posed to restrict the rotation in the lateral plane, also acting as dampers (Fig. 2). The tail mass was calculated by estimating the volume of the cylinders and multiplying it by the average density of flesh (1 kg/l), as in previous studies (Mallison 2015). The tail model is reconstructed with a total length of 264 cm and a total mass of 326.58 kg. The eleven pairs of caudal spines were hypothesised based on the whole tail being covered by spines, as in other stegosaur dinosaurs like *K. aethiopicus* (Costa & Mateus 2019). The addition to the model of the caudal spines increases its mass by an additional 138.7 kg, calculated considering the sum of the mass of cancellous, compact and keratin tissues that would have composed the caudal spine in life.

The dynamic and mathematical model of *M. longicollum* tail has been built in MBDyn (https://www.mbdyn.org/index.html), and the simulation results have been visualised in Blender, with the add-on Blendyn, by Andrea Zanoni.

The tail movement is imposed only on the first eight elements of the model of *M. longicollum* tail. The region corresponds to the front quarter of the model's length and is the zone where the largest musculature was present, according to previous studies (Carpenter et al. 2005; Conti et al. 2022). The motion was restricted to a single plane to save computing time, assuming that the tail musculature would be able to maintain the tail parallel to the ground. Each cosine function is tested at four different frequencies (1 Hz, 1.25 Hz, 1.5 Hz, and 2 Hz), with frequency serving as the sole variable across the four simulations. An applied stiffness value of $1.5*10^5$ N m/rad and a damping value of $3.5*10^4$ N m/rad ensure that the deformable joints maintain the model's integrity. Furthermore, the model is bound to a fixed element, corresponding with the sacrum in the animal, serving as a spatial constraint while running the simulation (Conti et al. 2022; see Supplementary Materials for the code of the model and simulation, S1). The model for the visual simulation was created using reference materials provided by Francisco Costa, incorporating photographic references and reconstructed models. These references include specimens

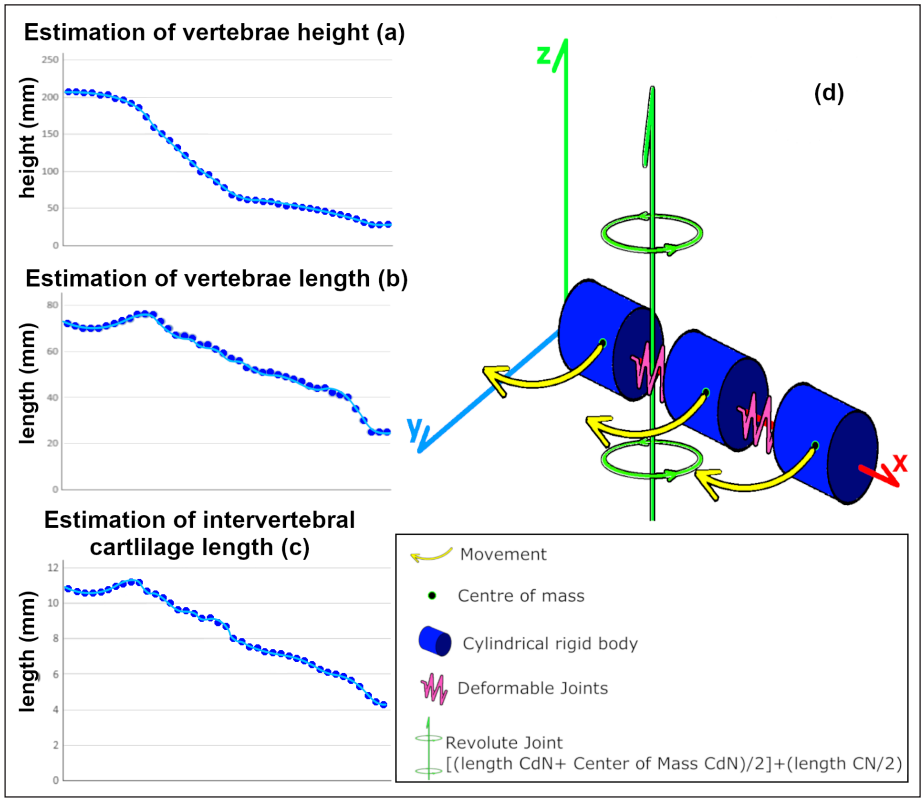

Fig. 2 - The graphs depict the caudal vertebrae height (a), length (b), development and the course of the intervertebral cartilage length (c). An illustration of the tail showing some vertebrae (cylinders) and cartilages (springs) (d). See text for further explanation.

like the *Kentrosaurus aethiopicus* from Berlin and the *Stegosaurus stenops* specimen NHMUK PV R36730. The impact forces produced by the model of the tail of *M. longicollum* were estimated following the approach of previous studies, based on other members of Thyreophora (Carpenter et al. 2005; Arbour 2009; Mallison 2011). The momentum generated by the movement of the tail model is calculated considering the total weight of 35.15 kg of the thagomizer (the most terminal caudal portion of the tail, which includes the last two pairs of caudal spines), and it is tested at the various velocities obtained from the MBDA simulations. Four different stopping times, obtained from the literature (Carpenter et al. 2005; Arbour 2009; Mallison 2011; Russel 2017) were used for the force calculus, ranging from $8.5*10^{-4}$ s up to 0.5 s. To enable comparison, the stress (σ) is calculated by dividing the Force by the impact area, which is kept constant at $2.8*10^{-5}$ m^2 (Carpenter et al. 2005).

The two morphologies of the caudal spines of *M. longicollum* and *S. stenops* were compared for their stress-bearing capabilities, since *M. longicollum* possesses caudal spines with a sigmoidal cross-section, different from the elliptical cross-section of *S. stenops*. The actual measurements obtained from the specimens MG 4863–39 (Costa & Mateus 2019) and NHMUK PV R36730 (Maidment et al. 2015) were used to reconstruct the proportion of the models of caudal spines, approximating mass and length by considering the characteristics of each component, including keratin (McKittrick et al. 2012), spongeous and compact bone. The two models were then compared assigning the same dimensions to test them. Data on the strength of bones were collected from different animals. The ultimate tensile strength was considered to range between 100 MPa and 210 MPa, data related to American alligator (*Alligator mississippiensis*) and Sarus crane (*Grus antigone*) bones (Currey 1987). The Poisson ratio employed for cortical bone in our study is 0.3, as reported in the article by Currey (1985). The ultimate compressive strength values were estimated at 170 MPa, obtained from data collected from ostrich bone samples (Conti et al. 2023) and 210 MPa from data collected from crocodile bone samples (Welgemoed 2018).

Results

MBDA simulation

The parameters of tail stiffness and damping were initially set at $1*10^4$ Nm/rad and $1*10^4$ Nm/rad respectively, to better emulate the natural movement. The mass of the caudal spines was later added to the

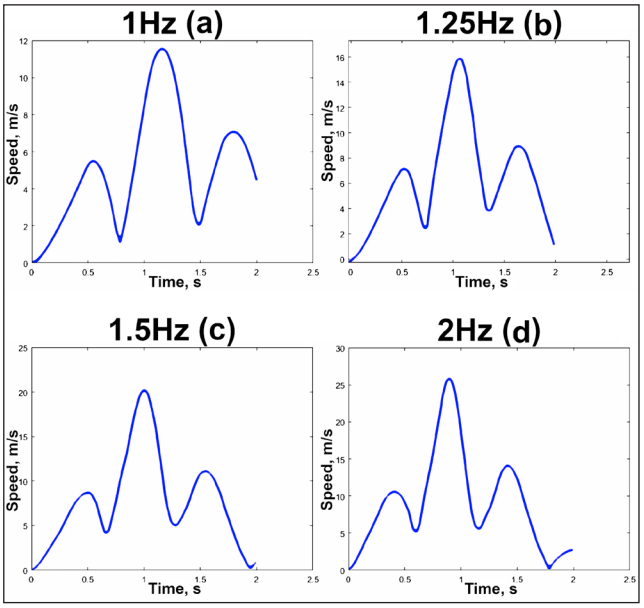

Fig. 3 - Speed of the tail tip in absolute values, reached by the four tests performed. (a) with 1.00 Hz, (b) with 1.25 Hz, (c) with 1.5 Hz and (d) with 2.00 Hz.

model and the frequency was increased. These modifications would lead to the failure of the simulation, as the joints would overextend beyond the imposed limits; a phenomenon that would correspond to the breaking of the animal's tail. To accommodate the new conditions, stiffness and damping parameters were increased to $1.5*10^5$ Nm/rad and $3.5*10^4$ Nm/rad, to maintain the integrity of the model and perform a complete simulation. The maximum velocity achievable is limited by the fixed base of the tail, representing the attachment of the tail to the body, which limits the angle of motion of the whole tail, as in the simulations performed on *K. aethiopicus* (Mallison et al. 2015). The simulation at the lowest frequency of 1Hz achieved a maximum velocity of 12 m/s (Fig. 3), with a 2 m displacement of the tail tip towards the animal's front and a 118° arc traversed by the tail (Fig. 4). The simulation performed with the frequency of 1.25 Hz attained a peak velocity of 17 m/s, a point-end displacement of 2.5 m, and a lateral arc of 148°. The third simulation with a frequency of 1.5 Hz achieved a peak velocity of 20 m/s (Fig. 3), reaching a point-end of nearly 3 m, and a 168° arc (Fig. 5). The fourth simulation with the highest frequency of 2 Hz reached a maximum velocity of 26 m/s (Fig. 3), with the point-end of the tail surpassing 3 m toward the front of the animal, covering a 198° arc (Fig. 5; see also Supplementary Material for the video of the simulation, S2).

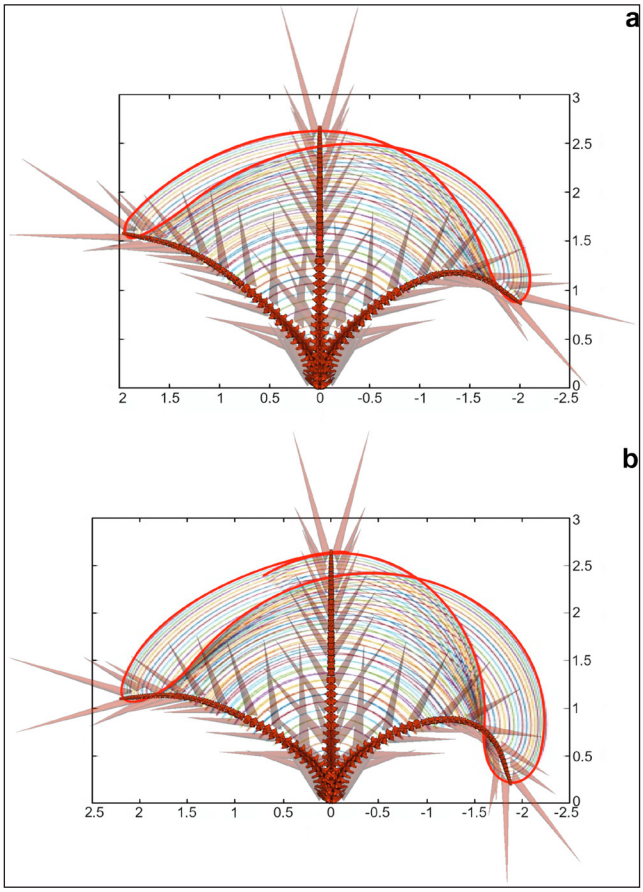

Fig. 4 - Path followed by the tail during the tests at (a) 12 m/s and (b) 17 m/s speed.

Force of impact

The whiplash of the tail model is calculated as an impulse (M) equivalent to the product obtained by multiplying the estimated total weight of 35.13 kg (m) of the thagomizer by the various velocities obtained from the MBDA (v); the obtained values range from 421.55 kg m/s to 913.36 kg m/s. The range of forces, calculated as the impulse (M) divided by the stopping time (sT), for the tail model, ranges from 0.84 kN, with a hypothetical stopping time of 0.5 s, up to 1074.54 kN, with the shortest stopping time of 0.00087s reported in the literature (Russell 2017). The stress (σ) ranges from 30 MPa to 38 GPa (Tab. 1).

Caudal spines (thagomizer) performances

We performed two stress tests for bending and compression of the caudal spines, using both a standardized length of 1 m for both taxa and the actual length of the fossil specimens (Fig. 6). For the caudal spines of 1 m in length, the bending test shows that *M. longicollum* caudal spines could

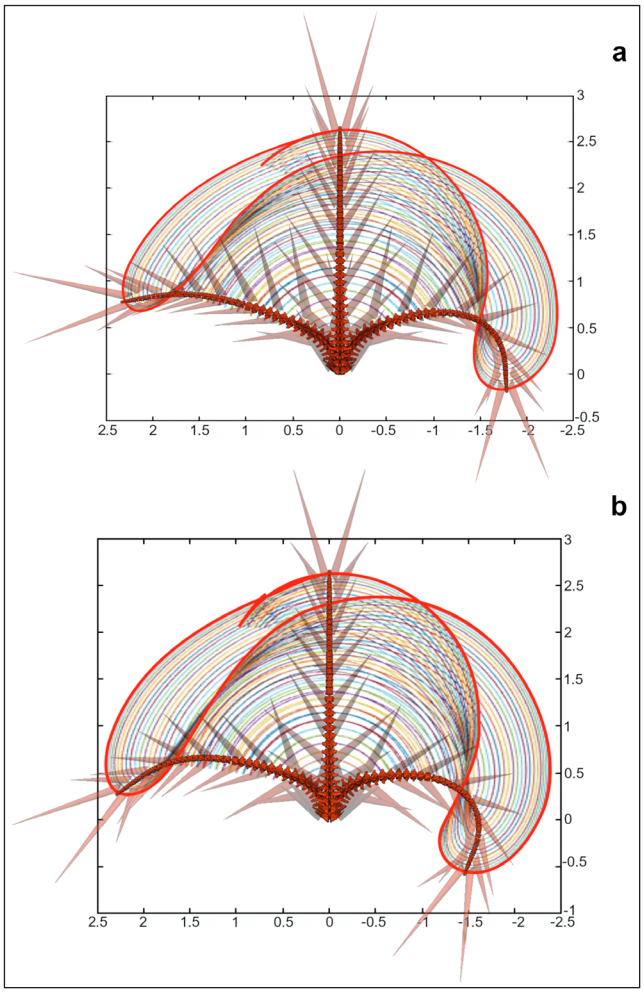

Fig. 5 - Path followed by the tail during the tests at: (a) 20 m/s and (b) 26 m/s speed.

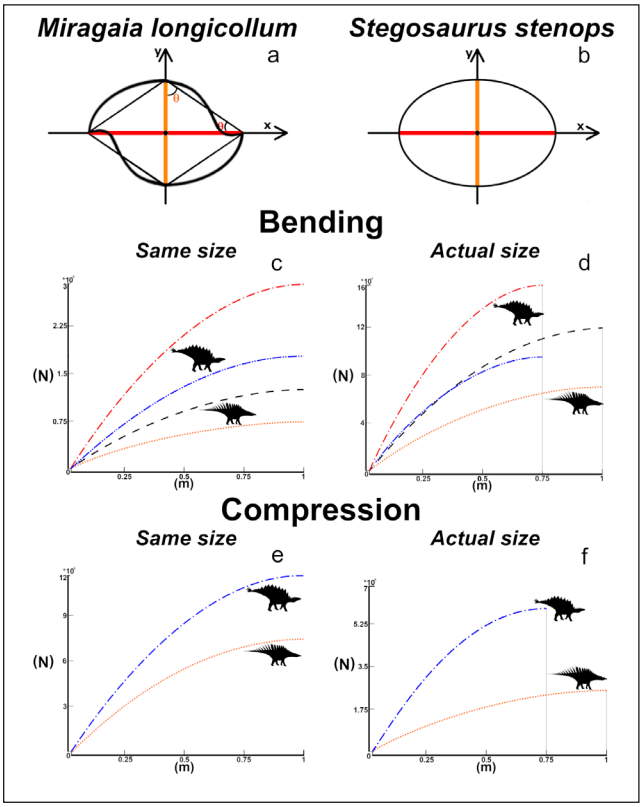

Fig. 6 - Shapes used for caudal spines bending and compression behaviours. Rhomboid section for *M. longicollum* (a) and ellipsoid for *S. stenops* (b). The minor axis is indicated in orange, while the major axis is shown in red. Graphs illustrating the bending (c, d) and compression (e, f) behaviour of the caudal spines of *M. longicollum* and *S. stenops*, respectively. The graphs on the left (c, e) depict the caudal spines tested at the same length (1 m), whereas the graphs on the right (d, f) show the caudal spines tested at their actual lengths (0.75 m for *S. stenops* and 1 m for *M. longicollum*).

bear stresses ranging from 11.70 N to 2.45 × 10^5 N around the minor axis, and from 6.9 N to 1.45 × 10^5 N around the major axis. In contrast, the caudal spines of *S. stenops* could bear stresses ranging from 28 N to 5.88 × 10^5 N around the minor axis, and from 17.11 N to 3.95 × 10^5 N around the major axis (Tab. 2). For the actual caudal spine sizes, the bending test shows that *M. longicollum* could bear loads ranging from 1.86 N to 3.91 × 10^4 N around the minor axis, and from 1.12 N to 2.35 × 10^4 N around the major axis. The caudal spines of *S. stenops* could bear higher stresses ranging from 4 N to 2.01 × 10^5 N around the minor axis, and from 2.42 N to 1.20 × 10^5 N around the major axis (Tab. 3).

For the spines length of 1 m, the compression test shows that *M. longicollum* caudal spines could bear stresses ranging from 1.68 × 10^4 N to 8.32 × 10^6 N, while *S. stenops* caudal spines could bear stresses ranging from 2.64 × 10^4 N to 1.31 × 10^7 N (Tab. 4). For the actual caudal spine sizes, *M. longicollum* might bear 4.90 × 10^3 N to 2.42 × 10^6 N, whereas *S. stenops* might bear 6.05 × 10^3 N to 5.31 × 10^6 N (Tab. 4). These results are illustrated in Fig. 6.

Discussion

The tails of stegosaurs possessed a greater degree of flexibility when compared to those of ankylosaurs (Arbour et al. 2018). In the event of a collision, the caudal spines on the stegosaur tail were designed to cleave through tissue instead of causing bone damage or tissue bruising (Carpenter et al. 2005). While the likelihood of internal organ damage was relatively low, the caudal spines could still inflict significant harm by slicing through skin and muscle, resulting in severe blood loss and muscle trauma (Gertsch 1994). Simulations indicate

	t stop (s)	Carpenter area *S.stenops* (m2)	Weight thagomizer *M. longicollum* (kg)	Weight thagomizer *S. stenops* (kg)	Speeds of the model (m/s)	Momentum m*V(kg*m/s) *M. longicollum*	Force J/t stop (kN) *M. longicollum*	Stress impact (MPa) *M. longicollum*	Stress impact of only 2 spines (MPa) *M. longicollum*	Momentum m*V(kg*m/s) *S. stenops*	Force J/t stop (kN) *S. stenops*	Stress impact (MPa) *S. stenops*	Stress impact of only 2 spines (MPa) *S. stenops*
Carpenter time	0.333	2.80E-05	35.13	14.00	12.00	421.55	1.27	45.21	22.61	168.00	0.50	18.02	9.01
Mallison time	0.05				17.00	597.20	1.79	64.05	32.02	238.00	0.71	25.53	12.76
Baseball bat time	0.00085				20.00	702.58	2.11	75.35	37.68	280.00	0.84	30.03	15.02
Optimistic time	0.5				26.00	913.36	2.74	97.96	48.98	364.00	1.09	39.04	19.52
							8.43	301.11	150.55		3.36	120.00	60.00
							11.94	426.57	213.28		4.76	170.00	85.00
							14.05	501.85	250.92		5.60	200.00	100.00
							18.27	652.40	326.20		7.28	260.00	130.00
							495.94	17712.20	8856.10		197.65	7058.82	3529.41
							702.58	25092.29	12546.14		280.00	10000.00	5000.00
							826.57	29520.34	14760.17		329.41	11764.71	5882.35
							1074.54	38376.44	19188.22		428.24	15294.12	7647.06
							0.84	30.11	15.06		0.34	12.00	6.00
							1.19	42.66	21.33		0.48	17.00	8.50
							1.41	50.18	25.09		0.56	20.00	10.00
							1.83	65.24	32.62		0.73	26.00	13.00

Tab. 1 - The table shows the calculus done using the different stopping times (Yellow=Carpenter; Orange=Mallison; Red=Baseball hitter; Green=Optimistic). See text for further explanation.

that *M. longicollum* might actively utilise its tail as a weapon for defence. However, they also demonstrate that the caudal spines' distinctive cross-sectional form is not as strong as those of its American equivalent, *S. stenops*.

MBDA modelling

The use of cutting-edge methods such as MBDA in biomechanical studies of stegosaurian tails, coupled with recent advancements in computer technology and its high performance, has not only enabled the exploration of questions that were previously unanswerable but has also significantly reduced the time required for comprehensive analysis compared to earlier methodologies. Although the model is a simulation and therefore a simplification of reality, the results presented in this paper provide a better understanding of the capabilities and dynamics of the tail of an extinct taxon. The mass estimated for the model (326.58 kg without the caudal spines, 465.28 kg including the spines) is comparable to Mallison's "slim" model of *K. aethiopicus* (Mallison 2011), pointing to a musculoskeletal system for the tail of *M. longicollum*.

Comparison with previous studies

The results obtained regarding the tension and pressures developed by the impact of the tail of *M. longicollum* presented in this study are congruent and follow the same approach as the one used in previous studies (Carpenter et al. 2005).

Impact Forces. In previous works, *S. stenops* was able to swing its tail up to exert 360-510 N of force, which is more than adequate to harm tissue and bone (Carpenter et al. 2005). This was demonstrated with an estimated spike-tip impact area of 2.8*10-5 m^2, resulting in an impact stress of 13-18 N/m^2 (Carpenter et al. 2005). Accordingly, since our simulations proved that the tail of *M. longicollum* could generate greater forces, we regard this evidence as more than adequate to generate pressure sufficient to damage soft tissues and shatter bones. Since the two thagomizers are different in weight (*M. longicollum* thagomizer weighing 35.15 kg, more than twice that of *S. stenops,* estimated at 14 kg; Carpenter et al. 2005), the differences in impact forces and thagomizer weight suggest *M. longicollum*'s tail was robust enough to deter predators. The forces developed by the impact of the tail of *M. longicollum* are smaller in comparison with the forces resulting from the previous study on *K. aethiopicus* (Mallison 2011). The main differences are related to the different stopping time values used in the two studies. The stopping time of 0.05 s for *K. aethiopicus* (Mallison 2011) is unlikely, considering that the collision would be anelastic and that the contact time increases with the increment of the involved masses (Hubbard et al. 1989). Accordingly, Mallison (2011) achieved higher pressures by applying a shorter stopping time than in previous studies (Arbour 2009; Carpenter et al. 2005), and those estimated in this study. According to our test *M. longicollum* whiplash could generate greater forces than that of *S. stenops*.

Tab. 2 - Bending tests for the caudal spines of *M. longicollum* and *S. stenops*, with the same sizes. See text for further explanation.

Bending tests with the same sizes

	Ultimate tensile strength (Pa)	Diameter 36/22	Lenght tested (m)	Section Major Axis (m)	Section Minor Axis (m)	Hypotenuse (m)	Hypo Simplified (m)	Sin Alpha	Theta (θ)	Inerzia (rombo) J = 1/3*Hypo^4*sin(Theta)^3*cos(Theta) (Theta angle of the axis of rotation)	F=100MPa	F =120 MPa	F=145MPa	F=210MPa
***M. longicollum* Spine Revolution around Minor Axis**		Base Spine	1	0.18	0.11	0.211	0.21	0.8571	59	2.10E-04	**1.17E+05**	**1.40E+05**	**1.69E+05**	**2.45E+05**
	120000000	At 1cm from tip	0.01	0.0018	0.0011	0.0021	0.0021	0.8571	59	2.09E-12	**1.16E+01**	**1.40E+01**	**1.69E+01**	**2.44E+01**
	145000000	at 25cm from tip	0.25	0.045	0.0275	0.0527	0.05	0.9	59	6.70E-07	**5.96E+03**	**7.15E+03**	**8.64E+03**	**1.25E+04**
	210000000	at 50cm from tip	0.5	0.09	0.0505	0.1032	0.1	0.9	59	1.08E-05	**2.40E+04**	**2.88E+04**	**3.48E+04**	**5.04E+04**
	100000000	at 60cm from tip	0.6	0.108	0.066	0.1266	0.12	0.9	59	2.24E-05	**3.46E+04**	**4.15E+04**	**5.02E+04**	**7.27E+04**
		at 80cm from tip	0.8	0.144	0.088	0.1688	0.17	0.8471	59	9.03E-05	**7.84E+04**	**9.41E+04**	**1.14E+05**	**1.65E+05**
	Ultimate tensile strength (Pa)	Diameter 36/22	Lenght tested (m)	Section Major Axis (m)	Section Minor Axis (m)	Hypotenuse (m)	Hypo Simplified (m)	Sin Alpha	Theta (θ)	Inerzia (rombo) J = 1/3*Hypo^4*sin(Theta)^3*cos(Theta) (Theta angle of the axis of rotation)	F=100MPa	F =120 MPa	F=145MPa	F=210MPa
***M. longicollum* Spine Revolution around Major Axis**		Base Spine	1	0.18	0.11	0.211	0.21	0.5238	31	7.59E-05	**6.90E+04**	**8.28E+04**	**1.00E+05**	**1.45E+05**
	120000000	At 1cm from tip	0.01	0.0018	0.0011	0.0021	0.0021	0.5238	31	7.59E-13	**6.90E+00**	**8.28E+00**	**1.00E+01**	**1.45E+01**
	145000000	at 25cm from tip	0.25	0.045	0.0275	0.0527	0.05	0.55	31	2.44E-07	**3.55E+03**	**4.26E+03**	**5.15E+03**	**7.45E+03**
	210000000	at 50cm from tip	0.5	0.09	0.0505	0.1032	0.1	0.505	31	3.90E-06	**1.54E+04**	**1.85E+04**	**2.24E+04**	**3.24E+04**
	100000000	at 40cm from tip	0.6	0.108	0.066	0.1266	0.12	0.55	31	8.09E-06	**2.04E+04**	**2.45E+04**	**2.96E+04**	**4.29E+04**
		at 20cm from tip	0.8	0.144	0.088	0.1688	0.17	0.5176	31	3.26E-05	**4.63E+04**	**5.56E+04**	**6.72E+04**	**9.73E+04**
	Ultimate tensile strength (Pa)	Diameter 36/22	Lenght tested (m)	Section Major Axis (m)	Section Minor Axis (m)	Hypotenuse (m)	Hypo Simplified (m)	Sin Alpha	Theta (θ)	Inerzia (Ellipse) J = (π/4)* (Major Axis^3) * (Minor Axis)	F=100MPa	F =120 MPa	F=145MPa	F=210MPa
***S. stenops* Spine Revolution around Minor Axis**		Base Spine	1	0.18	0.11	0.211	0.21	0.8571	59	5.04E-04	**2.80E+05**	**3.36E+05**	**4.06E+05**	**5.88E+05**
	120000000	At 1cm from tip	0.01	0.0018	0.0011	0.0021	0.0021	0.8571	59	5.04E-12	**2.80E+01**	**3.36E+01**	**4.06E+01**	**5.88E+01**
	145000000	at 25cm from tip	0.25	0.045	0.0275	0.0527	0.05	0.9	59	1.97E-06	**1.75E+04**	**2.10E+04**	**2.54E+04**	**3.67E+04**
	210000000	at 50cm from tip	0.5	0.09	0.0505	0.1032	0.1	0.9	59	2.89E-05	**6.43E+04**	**7.71E+04**	**9.32E+04**	**1.35E+05**
	100000000	at 60cm from tip	0.6	0.108	0.066	0.1266	0.12	0.9	59	6.53E-05	**1.01E+05**	**1.21E+05**	**1.46E+05**	**2.12E+05**
		at 80cm from tip	0.8	0.144	0.088	0.1688	0.17	0.8471	59	2.06E-04	**1.79E+05**	**2.15E+05**	**2.60E+05**	**3.76E+05**
	Bending around major axis	Diameter 36/22	Lenght tested (m)	Section Major Axis (m)	Section Minor Axis (m)	Hypotenuse (m)	Hypo Simplified (m)	Sin Alpha	Theta (θ)	Inerzia (Ellipse) J = (π/4)* (Major Axis) * (Minor Axis^3)	F=100MPa	F =120 MPa	F=145MPa	F=210MPa
***S. stenops* Spine Revolution around Major Axis**		Base Spine	1	0.18	0.11	0.211	0.21	0.5238	31	1.88E-04	**1.71E+05**	**2.05E+05**	**2.48E+05**	**3.59E+05**
	120000000	At 1cm from tip	0.01	0.0018	0.0011	0.0021	0.0021	0.5238	31	1.88E-12	**1.71E+01**	**2.05E+01**	**2.48E+01**	**3.59E+01**
	145000000	at 25cm from tip	0.25	0.045	0.0275	0.0527	0.05	0.55	31	7.35E-07	**1.07E+04**	**1.28E+04**	**1.55E+04**	**2.25E+04**
	210000000	at 50cm from tip	0.5	0.09	0.0505	0.1032	0.1	0.505	31	9.10E-06	**3.61E+04**	**4.33E+04**	**5.23E+04**	**7.57E+04**
	100000000	at 60cm from tip	0.6	0.108	0.066	0.1266	0.12	0.55	31	2.44E-05	**6.16E+04**	**7.39E+04**	**8.93E+04**	**1.29E+05**
		at 80cm from tip	0.8	0.144	0.088	0.1688	0.17	0.5176	31	7.71E-05	**1.09E+05**	**1.31E+05**	**1.59E+05**	**2.30E+05**

The differences in pressure levels attained (75.35 MPa for *M.longicollum,* compared to about 150 MPa for *K. aethiopicus* in Mallison 2011) might be related to the different geometries of caudal spines considered and the heavier thagomizer and slower speeds used for *M. longicollum.* The variations in the geometry of the spines could affect the use of the thagomizer as a weapon or as a defensive tool since different geometries confer to the spines different responses when solicited by bending and compression forces. A previous simulation with the unique tail structure of *K. aethiopicus* proved that even with the lowest mass estimation of the tail ('slim' model), *K. aethiopicus* could deliver high-pressure strikes even at relatively modest speeds (Mallison 2011). Such adaptation allowed *K. aethiopicus* to wield its tail as a defence mechanism, capable of causing significant harm or deterrence. In contrast with the reconstruction of *K. aethiopicus*, *M. longicollum*'s tail featured a cluster of multiple tail caudal spines. The presence of a heavier thagomizer confers the capacity to achieve higher velocities and higher impact forces than *K. aethiopicus*. Despite the fewer caudal spines, implying less surface involved during the impact, generated pressures would still be sufficient to cause harm, hence being used as weapons. The comparative analysis of tail defensive mechanisms in *M. longicollum* and ankylosaurian dinosaurs elucidates both convergent evolutionary patterns and distinct adaptations. Ankylosaurs exhibited robust tail knobs capable of delivering formidable, bone-breaking blows to predators, as evidenced by UALVP 16247, which represents average knob width and could impact with a force of 962–2014 N, exerting an impact stress of 4811–10 070 N/cm^2 (48–100 MPa) (Arbour & Sniveley 2009). However, these figures may underestimate the true impact forces and stresses in average-sized knobs, potentially enabling them to break bone during impacts. In contrast, while effective, *M. longicollum*'s thagomizer operated at a comparatively lower impact potential. Furthermore, the comparison was prompted by the structural similarity between *M. longicollum*'s thagomizer and ankylosaurian tail knobs. The enlarged base of the caudal spines in *M. longicollum*'s thagomizer forms a structure resembling a tail knob, suggesting convergent evolution in tail defence strategies. Moreover, the diverse range of tail structures

Tab. 3 - Bending tests for the caudal spines of *M. longicollum* and *S. stenops* with their actual sizes. See text for further explanation.

Bending tests with actual sizes

***M. longicollum* Spine Revolution around Minor Axis**	Ultimate tensile strength (Pa)	Diameter 18/11	Lenght tested (m)	Section Major Axis (m)	Section Minor Axis (m)	Hypotenuse (m)	Hypo Simplified (m)	Sin Alpha	Theta (θ)	Inerzia (rombo) J = 1/3*Hypo^4*sin(Theta)^3*cos(Theta) (Theta angle of the axis of rotation)	F =100MPa	F =120MPa	F =145MPa	F =210MPa
		Base Spine	1	0.098	0.0588	0.1143	0.114	0.8596	59	1.83E-05	**18634.09**	**22360.91**	**27019.4**	**39131.6**
	1.2E+08	At 1cm from tip	0.01	0.001	0.0006	0.0011	0.0011	0.8596	59	1.82E-13	**0.018565**	**0.022278**	**0.02692**	**0.03899**
	1.45E+08	at 25cm from tip	0.25	0.0245	0.0147	0.0286	0.028	0.875	59	6.65E-08	**271.257**	**325.5084**	**393.323**	**569.64**
	2.1E+08	at 50cm from tip	0.5	0.049	0.0294	0.0571	0.057	0.8575	59	1.14E-06	**2329.261**	**2795.114**	**3377.43**	**4891.45**
	1E+08	at 40cm from tip	0.6	0.0588	0.0353	0.0686	0.068	0.8575	59	2.31E-06	**3931.635**	**4717.962**	**5700.87**	**8256.43**
		at 20cm from tip	0.8	0.0784	0.047	0.0914	0.091	0.8575	59	7.41E-06	**9457.239**	**11348.69**	**13713**	**19860.2**
***M. longicollum* Spine Revolution around Major Axis**	Ultimate tensile strength (Pa)	Diameter 18/11	Lenght tested (m)	Section Major Axis (m)	Section Minor Axis (m)	Hypotenuse (m)	Hypo Simplified (m)	Sin Alpha	Theta (θ)	Inerzia (rombo) J = 1/3*Hypo^4*sin(Theta)^3*cos(Theta) (Theta angle of the axis of rotation)	F =100MPa	F =120MPa	F =145MPa	F =210MPa
		Base Spine	1	0.098	0.0588	0.1143	0.114	0.5158	31	6.59E-06	**11212.55**	**13455.06**	**16258.2**	**23546.4**
		At 1cm from tip	0.01	0.001	0.0006	0.0011	0.0011	0.5158	31	6.59E-14	**0.011213**	**0.013455**	**0.01626**	**0.02355**
		at 25cm from tip	0.25	0.0245	0.0147	0.0286	0.028	0.525	31	2.40E-08	**163.2214**	**195.8657**	**236.671**	**342.765**
		at 50cm from tip	0.5	0.049	0.0294	0.0571	0.057	0.5158	31	4.12E-07	**1401.569**	**1681.883**	**2032.27**	**2943.29**
		at 40cm from tip	0.6	0.0588	0.0353	0.0686	0.068	0.5188	31	8.35E-07	**2365.753**	**2838.904**	**3430.34**	**4968.08**
		at 20cm from tip	0.8	0.0784	0.047	0.0914	0.091	0.5169	31	2.68E-06	**5690.633**	**6828.76**	**8251.42**	**11950.3**
***S. stenops* Spine Revolution around Minor Axis**	Bending around minor axis	Diameter 22/14	Lenght tested (m)	Section Major Axis (m)	Section Minor Axis (m)	Hypotenuse (m)	Hypo Simplified (m)	Sin Alpha	Theta (θ)	Inerzia (Ellipse) J = (π/4)* (Major Axis^3) * (Minor Axis)	F =100MPa	F =120MPa	F =145MPa	F =210MPa
		Base Spine	0.75	0.115	0.069	0.1341	0.114	0.6053	59	8.24E-05	**95559.39**	**114671.3**	**138561**	**200675**
		At 0,075cm from tip	0.0075	0.0009	0.0005	0.001	0.0011	0.4539	59	2.61E-13	**4.031412**	**4.837694**	**5.84555**	**8.46597**
		at 18,75cm from tip	0.1875	0.0216	0.0129	0.0251	0.028	0.4621	59	1.02E-07	**2519.632**	**3023.559**	**3653.47**	**5291.23**
		at 37,5cm from tip	0.375	0.0431	0.0259	0.0503	0.057	0.4539	59	1.63E-06	**10078.53**	**12094.24**	**14613.9**	**21164.9**
		at 30cm from tip	0.45	0.0518	0.0311	0.0604	0.068	0.4566	59	3.38E-06	**14513.08**	**17415.7**	**21044**	**30477.5**
		at 15cm from tip	0.6	0.069	0.0414	0.0805	0.091	0.4549	59	1.07E-05	**25801.04**	**30961.24**	**37411.5**	**54182.2**
***S. stenops* Spine Revolution around Major Axis**	Bending around major axis	Diameter 22/14	Lenght tested (m)	Section Major Axis (m)	Section Minor Axis (m)	Hypotenuse (m)	Hypo Simplified (m)	Sin Alpha	Theta (θ)	Inerzia (Ellipse) J = (π/4)* (Major Axis) * (Minor Axis^3)	F =100MPa	F =120MPa	F =145MPa	F =210MPa
		Base Spine	0.75	0.115	0.069	0.1341	0.114	0.5158	31	2.97E-05	**57335.64**	**68802.76**	**83136.7**	**120405**
		At 0,0075cm from tip	0.0075	0.0009	0.0005	0.001	0.0011	0.5158	31	9.39E-14	**2.418847**	**2.902617**	**3.50733**	**5.07958**
		at 18,75cm from tip	0.1875	0.0216	0.0129	0.0251	0.028	0.525	31	3.67E-08	**1511.779**	**1814.135**	**2192.08**	**3174.74**
		at 37,5cm from tip	0.375	0.0431	0.0259	0.0503	0.057	0.5158	31	5.87E-07	**6047.118**	**7256.542**	**8768.32**	**12698.9**
		at 40cm from tip	0.45	0.0518	0.0311	0.0604	0.068	0.5188	31	1.22E-06	**8707.85**	**10449.42**	**12626.4**	**18286.5**
		at 55cm from tip	0.6	0.069	0.0414	0.0805	0.091	0.5169	31	3.85E-06	**15480.62**	**18576.75**	**22446.9**	**32509.3**

among ankylosaurians exemplifies their adaptive versatility. The systematic consideration of stopping time in force calculations unveils fundamental principles governing the biomechanics of tail-based defence mechanisms. This highlights the efficacy of the swing of the knob and the thagomizer as defensive tools.

Bending and Compression

To estimate the stress resistance capabilities of *M. longicollum* caudal spines to bending and compressional loads, we compared them to the caudal spine capabilities of *S. stenops* (Tabs. 2-4). When running the test on spines with the same sizes for the two taxa, *S. stenops* caudal spines showed to be capable of reaching higher pressures in bending and compression. Moreover, the data show that despite *S. stenops* spines are shorter than *M. longicollum* ones, they can withstand higher bending stresses compared to *M. longicollum* (difference of $1.75*10^5$ N on the major axis and $1*10^5$ N on the minor axis). The same trend can be observed under compressional stresses, with *S. stenops* spines being able to sustain 5 MPa higher stress than *M. longicollum*. Thus, *S. stenops*' caudal spines are sturdier and better at withstanding impact stresses. As shown by the results, the elliptical cross-section shape of *S. stenops* caudal spines proves superior in bearing bending and compression, compared to the sigmoid cross-section shape of *M. longicollum* caudal spines. (Tabs 1-3).

Further implications

Due to the lack of knowledge on the orientation and number of caudal spines of *M. longicollum*, two hypotheses were tested: the first, with an orientation similar to the reconstruction of *K. aethiopicus* (Mallison 2011), characterized by an upward orientation and maintaining the same angle to the dorsoventral axis and the same lateral inclination; the second design with the caudal spines disposed of

Compression tests with the same sizes — a

Pressure point	Lenght (m)	Section Major Axis (m)	Section Minor Axis (m)	*M. longicollum spines Area (m2) (rhombus)*	*S. stenops spine Area (m2) (ellipse)*	Ultimate Compressive Strength (MPa) (Realistic)	Ultimate Compressive Strength (MPa) (Best Hypothesis)	Force (N) = Ultimate Compressive Strength*Area (M. longicollum - Realistic)	Force (N) = Ultimate Compressive Strength*Area (M. longicollum - Best Hypothesis)	Force (N) = Ultimate Compressive Strength*Area (S. stenops - Realistic)	Force (N) = Ultimate Compressive Strength*Area (S. stenops - Best Hypothesis)
Base Spine	1	0.18	0.11	0.0396	0.0622	1.7E+08	2.1E+08	**6732000**	**8316000**	**10574600.9**	**13062742.3**
At 5cm from tip	0.05	0.009	0.0055	0.0001	0.00016	1.7E+08	2.1E+08	**16830**	**20790**	**26436.5022**	**32656.8556**
At 10cm from tip	0.1	0.018	0.011	0.0004	0.00062	1.7E+08	2.1E+08	**67320**	**83160**	**105746.009**	**130627.423**
At 25cm from tip	0.25	0.045	0.0275	0.00248	0.00389	1.7E+08	2.1E+08	**420750**	**519750**	**660912.555**	**816421.391**
At 50cm from tip	0.5	0.09	0.0505	0.00909	0.01428	1.7E+08	2.1E+08	**1545300**	**1908900**	**2427351.56**	**2998493.11**

Compression tests with actual sizes — b

	M. longicollum Spines Pressure point	Lenght (m)	Section Major Axis (m)	Section Minor Axis (m)	*M. longicollum* spines Area (m2) (rhombus)	Ultimate Compressive Strength (MPa) (Realistic)	Ultimate Compressive Strength (MPa) (Best Hypothesis)	Force (N) = Ultimate Compressive Strength*Area (*M. longicollum* Realistic)	Force (N) = Ultimate Compressive Strength*Area (*M. longicollum* - Best Hypothesis)
M. longicollum	**Base Spine**	1	0.098	0.0588	0.011525	170000000	210000000	**1959216**	**2420208**
	At 5cm from tip	0.05	0.0049	0.00294	0.000029			**4898.04**	**6050.52**
	at 10cm from tip	0.1	0.0098	0.00588	0.000115			**19592.16**	**24202.08**
	at 25cm from tip	0.25	0.0245	0.0147	0.00072			**122451**	**151263**
	at 50cm from tip	0.5	0.049	0.0294	0.002881			**489804**	**605052**
	S. stenops Spines Pressure point	Lenght (m)	Section Major Axis (m)	Section Minor Axis (m)	*S. stenops* spine Area (m2) (ellipse)	Ultimate Compressive Strength (MPa) (Realistic)	Ultimate Compressive Strength (MPa) (Best Hypothesis)	Force (N) = Ultimate Compressive Strength*Area (*S. stenops* - Realistic)	Force (N) = Ultimate Compressive Strength*Area (*S. stenops* -Best Hypothesis)
S. stenops	**Base Spine**	0.75	0.115	0.07	0.02529	170000000	210000000	**4299269.55**	**5310862.381**
	At 0,0375cm from tip	0.0375	0.00431	0.00263	0.00004			**6045.8478**	**7468.400223**
	at 7,5cm from tip	0.075	0.00863	0.00525	0.00014			**24183.3912**	**29873.60089**
	at 18,75cm from tip	0.1875	0.02156	0.01313	0.00089			**151146.195**	**186710.0056**
	at 37,5cm from tip	0.375	0.04313	0.02625	0.00356			**604584.78**	**746840.0223**

Tab. 4 - (a) Results obtained with the same size during the compression tests; (b) results with their actual size.

with a high lateral angle (see Supplementary Materials, S3). The first orientation of the caudal spines might increase the tail's striking range and perhaps inflict slashing damage on approaching predators. The second orientation may confer a more penetrative capability but also it would demand a larger tail musculature, capable of exerting greater control over the movement of the tail. Despite having run the simulations in both configurations, no distinguishable results could have been discerned, suggesting that the orientation of the spines does not deeply affect the dynamic of the motion of the tail.

The high number of caudal spines suggested for *M. longicollum* supports the two different orientations hypothesized here (Costa & Mateus 2019). In addition, such a high number might suggest that caudal spines were not just used as weapons; they might have complemented the function of dorsal plates as a deterrent to predators, acting as a protection from attack from behind, and for intraspecific behaviours, such as mating and territorial struggle, and be a feature of sexual dimorphism (Marsh 1877; Christiansen & Tschopp 2010 and references therein; Arbour et al. 2022).

Conclusion

Palaeontologists are increasingly using digitalization and digital analysis of fossils to study uni-

que specimens or specimens challenging to handle. Digital models make it possible to easily examine fossil samples and specimens in places other than their storage location, enabling damage-free inspection of even the most delicate items. The use of software for biomechanics and the reconstruction of real-world models has increased significantly since the start of the century. In this work, we have presented the application of 3D modelling to the reconstruction and simulation of creatures' movements with MBDA. In this context, the technique has been applied to the study and reconstruction of the tail of *M. longicollum* and the evaluation of its defensive capabilities. The bending and compression data obtained for its caudal spines have provided valuable insights into the diversity of function and behaviour of the tail and thagomizer of stegosaurian dinosaurs.

Based on the simulation, the estimated mass of the tail model suggests the presence of a robust musculoskeletal system evolved to support and control the tail movement. The significant weight calculated for the model, supporting a muscular tail or a musculoskeletal system, shows that *M. longicollum* could have used the tail as a weapon.

The simulations indicate that while *M. longicollum*'s caudal spines are less robust than those of *S. stenops*, they suggest a multifaceted functional role. The sheer visual impact of these spines could effectively deter predators, avoiding confrontations. Additionally, the spines likely played a significant role in social interactions, such as mating rituals or dominance displays, signalling fitness or status within the species. This visual display would be crucial for intra-species communication, influencing mate selection and hierarchical structures. Furthermore, the arrangement of the numerous spines might have created a formidable protective barrier, making it challenging for predators to approach and attack vulnerable body parts. The presence of numerous spines, if confirmed by future findings, points to a strategy that prioritizes intimidation over direct physical combat. Moreover, future studies could address if *M. longicollum* employed lateral movement of the whole body to increase the momentum of the tail swing, instead of a more muscular tail as shown in the present study.

Acknowledgements: The authors thank Francisco Costa for the knowledge and photographic material shared regarding the caudal spines' anatomy and the *Miragaia longicollum*'s reconstruction. The authors also thank Prof. Pierangelo Masarati and Andrea Zanoni for their help with running the simulations and the use of the software MBDyn. Thoroughly review of two anonymous reviewers has greatly improved the quality of this manuscript.

References

Arbour V.M. (2009) - Estimating impact forces of tail club strikes by ankylosaurid dinosaurs. *PLoS ONE,* 4, e6738.

Arbour V.M. & Zanno L.E. (2018) - The evolution of tail weaponization in amniotes. *Proceedings of the Royal Society B: Biological Sciences*, 285(1871), 20172299.

Arbour V.M., Zanno L.E. & Evans D.C. (2022) - Palaeopathological evidence for intraspecific combat in ankylosaurid dinosaurs. *Biology Letters*, 18(12), 20220404.

Averianov A.O. & Krasnolutskii S.A. (2009) - Stegosaur remains from the Middle Jurassic of west Siberia. *Trudy Zoologicheskogo instituta RAN*, 313(2): 153-167.

Carpenter K., Sanders F., Mc Whinney L.A. & Wood L. (2005) - Evidence for predator-prey relationships. In: Carpenter K. (Ed.) -The carnivorous dinosaurs: 325-350. Indiana University Press, Bloomington.

Christiansen N.A. & Tschopp E. (2010) - Exceptional stegosaur integument impressions from the Upper Jurassic Morrison Formation of Wyoming. *Swiss Journal of Geosciences,* 103: 163-171.

Conti S., Sala G. & Mateus O. (2023) - Smart biomechanical adaptation revealed by the structure of ostrich limb bones. *Biomimetics*, 8(1), 98.

Conti S., Tschopp E., Mateus O., Zanoni A., Masarati P. & Sala G. (2022) - Multibody analysis and soft tissue strength refute supersonic dinosaur tail. *Scientific Reports*, 12(1), 19245.

Costa F. & Mateus O. (2019) - Dacentrurine stegosaurs (Dinosauria): A new specimen of *Miragaia longicollum* from the Late Jurassic of Portugal resolves taxonomical validity and shows the occurrence of the clade in North America. *PloS one*, 14(11), e0224263.

Curtis N., Kupczik K., O'Higgins P., Moazen M. & Fagan M. (2008) - Predicting skull loading: applying multibody dynamics analysis to a macaque skull. *Anatomical Record,* 291; 491–501.

Díez Díaz V., Demuth O.E., Schwarz D. & Mallison H. (2020) - The tail of the Late Jurassic sauropod *Giraffatitan brancai*: digital reconstruction of its epaxial and hypaxial musculature, and implications for tail biomechanics. *Frontiers in Earth Sciences*, 8, 160.

Dong Z. (1983) - The dinosaurian remains from Sichuan basin, China. *Palaeontologia Sinica, new series C*, 23: 1-145.

Galton P.M. & Ayyasami K. (2017) - Purported latest bone of a plated dinosaur (Ornithischia: Stegosauria), a "dermal plate" from the Maastrichtian (Upper Cretaceous) of southern India. *Neues Jahrbuch fur Geologie und Palaontologie*, 285(1): 91-96.

Gertsch L. & Nelson G.E. (1994) - Dinosaur tail dynamics. In: Nelson G.E. (Ed.) - The Dinosaurs of Wyoming; 44th Annual Field Conference Guidebook: 25-38. Wyoming Geological Association, Casper.

Gilmore C.W. (1914) - Osteology of the armored Dinosauria in the United States National Museum: with special reference to the genus *Stegosaurus*. *Smithsonian Institution Bulletin*, 89: 1-122.

Hubbard M., Covarrubias J.R., Hagenau W. & Jenssen C. (1989) - Ball impact mechanics: biomechanical implications. *Journal of Biomechanics*, 22(10), 1027.

Jia L., Li N., Dong L., Shi J., Kang Z., Wang S., Xu S. & You H. (2024) - A new stegosaur from the late Early Cretaceous of Zuoyun, Shanxi Province, China. *Historical Biology*, 1-10.

Kang H. (2013) - The prevention and handling of the missing data. *Korean journal of anesthesiology*, 64(5), 402.

Langenbach G.E.J., Zhang F., Herring S.W. & Hannam A.G. (2002) - Modelling the masticatory biomechanics of a pig. *Journal of Anatomy,* 201: 383-393.

Lautenschlager S. (2020) - Multibody dynamics analysis (MDA) as a numerical modelling tool to reconstruct the function and palaeobiology of extinct organisms. *Palaeontology,* 63: 703-715.

Li N., Li D., Peng G. & You H. (2024) - The first stegosaurian dinosaur from Gansu Province, China. *Cretaceous Research*, 158, 105852.

Maidment S.C.R., Brassey C. & Barrett P.M. (2015) - The postcranial skeleton of an exceptionally complete individual of the plated dinosaur *Stegosaurus stenops* (Dinosauria: Thyreophora) from the Upper Jurassic Morrison Formation of Wyoming, U.S.A. *PLoS ONE* 10, e0138352.

Mallison H. (2011) - Defense capabilities of *Kentrosaurus aethiopicus* Hennig, 1915. *Palaeontologia Electronica* 14(2): 1-25.

Mallison H., Pittman M. & Schwarz D. (2015) - Using crocodilian tails as models for dinosaur tails. *PeerJ PrePrints,* e1653.

Marsh O.C. (1877) - A new order of extinct Reptilia (Stegosauria) from the Jurassic of the Rocky Mountains. *American Journal of Science*, 3(84): 513-514.

Mateus O., Maidment S.C.R. & Christiansen N.A. (2009) - A new long-necked 'sauropod-mimic' stegosaur and the evolution of the plated dinosaurs. *Proceedings of the Royal Society B,* 276: 1815–1821.

McKittrick J., Chen P.Y., Bodde S.G. Yang W., Novitskaya E. E. & Meyers M.A. (2012) - The structure, functions, and mechanical properties of keratin. *The Journal of The Minerals, Metals & Materials Society*, 64: 449-468.

Moazen M., Curtis N., Evans S.E., O'Higgins P. & Fagan M.J. (2008) - Combined finite element and multibody dynamics analysis of biting in a *Uromastyx hardwickii* lizard skull. *Journal of Anatomy*, 213(5): 499-508.

Russel D. (2017) - Acoustics and vibration of baseball and softball bats. *Acoust Today*, 13(4): 35-42.

Van Bijlert P.A., van Soest A.K. & Schulp A.S. (2021) - Natural Frequency Method: estimating the preferred walking speed of *Tyrannosaurus rex* based on tail natural frequency. *Royal Society open science*, 8(4), 201441.

Welgemoed L.A. (2018) - An experimental investigation of interspecies variation in mechanical properties of cortical bone. University of Cape Town Master Thesis: 1-156.

Zafaty O., Oukassou M., Riguetti F., Company J., Bendrioua S., Tabuce R., Charrière A. & Pereda-Suberbiola X. (2024) - A new stegosaurian dinosaur (Ornithischia: Thyreophora) with a remarkable dermal armour from the Middle Jurassic of North Africa. *Gondwana Research*, 131: 344-362.

External link

https://github.com/zanoni-mbdyn/blendyn